



**HAL**  
open science

## Large Intercalation Pseudocapacitance in 2D VO<sub>2</sub>(B): Breaking through the Kinetic Barrier

Chuan Xia, Zifeng Lin, Yungang Zhou, Chao Zhao, Hanfeng Liang, Patrick Rozier, Zhiguo Wang, Husam N. Alshareef

► **To cite this version:**

Chuan Xia, Zifeng Lin, Yungang Zhou, Chao Zhao, Hanfeng Liang, et al.. Large Intercalation Pseudocapacitance in 2D VO<sub>2</sub>(B): Breaking through the Kinetic Barrier. *Advanced Materials*, 2018, 30 (40), pp.1803594. 10.1002/adma.201803594 . hal-02351758

**HAL Id: hal-02351758**

**<https://hal.science/hal-02351758>**

Submitted on 6 Nov 2019

**HAL** is a multi-disciplinary open access archive for the deposit and dissemination of scientific research documents, whether they are published or not. The documents may come from teaching and research institutions in France or abroad, or from public or private research centers.

L'archive ouverte pluridisciplinaire **HAL**, est destinée au dépôt et à la diffusion de documents scientifiques de niveau recherche, publiés ou non, émanant des établissements d'enseignement et de recherche français ou étrangers, des laboratoires publics ou privés.





## Open Archive Toulouse Archive Ouverte (OATAO)

OATAO is an open access repository that collects the work of Toulouse researchers and makes it freely available over the web where possible

This is an author's version published in: <http://oatao.univ-toulouse.fr/24666>

**Official URL:** <https://doi.org/10.1002/adma.201803594>

### **To cite this version:**

Xia, Chuan and Lin, Zifeng  and Zhou, Yungang and Zhao, Chao and Liang, Hanfeng and Rozier, Patrick  and Wang, Zhiguo and Alshareef, Husam N. *Large Intercalation Pseudocapacitance in 2D VO<sub>2</sub>(B): Breaking through the Kinetic Barrier*. (2018) *Advanced Materials*, 30 (40). 1803594. ISSN 0935-9648

Any correspondence concerning this service should be sent to the repository administrator: [tech-oatao@listes-diff.inp-toulouse.fr](mailto:tech-oatao@listes-diff.inp-toulouse.fr)

# Large Intercalation Pseudocapacitance in 2D VO<sub>2</sub> (B): Breaking through the Kinetic Barrier

Chuan Xia, Zifeng Lin, Yungang Zhou, Chao Zhao, Hanfeng Liang, Patrick Rozier, Zhiguo Wang, and Husam N. Alshareef\*

**VO<sub>2</sub> (B) features two lithiation/delithiation processes, one of which is kinetically facile and has been commonly observed at 2.5 V versus Li/Li<sup>+</sup> in various VO<sub>2</sub> (B) structures. In contrast, the other process, which occurs at 2.1 V versus Li/Li<sup>+</sup>, has only been observed at elevated temperatures due to large interaction energy barrier and extremely sluggish kinetics. Here, it is demonstrated that a rational design of atomically thin, 2D nanostructures of VO<sub>2</sub> (B) greatly lowers the interaction energy and Li<sup>+</sup>-diffusion barrier. Consequently, the kinetically sluggish step is successfully enabled to proceed at room temperature for the first time ever. The atomically thin 2D VO<sub>2</sub> (B) exhibits fast charge storage kinetics and enables fully reversible uptake and removal of Li ions from VO<sub>2</sub> (B) lattice without a phase change, resulting in exceptionally high performance. This work presents an effective strategy to speed up intrinsically sluggish processes in non-van der Waals layered materials.**

Electrochemical capacitors have attracted significant interest recently due to their potential applications in portable and wearable electronics, electric vehicles, and even power grids.<sup>[1]</sup> There are usually three types of capacitive energy storage mechanisms in electrochemical capacitors: double-layer capacitance, surface Faradic pseudocapacitance, and intercalation pseudocapacitance.<sup>[2]</sup> Electrical double-layer capacitors (EDLCs) are based

on the electrosorption of ions at the interface between electrode materials, typically carbon, and electrolytes. In spite of their excellent rate capability and robust cycling performance, EDLCs are known to suffer from low energy density, which limits their practical applications. On the other hand, intrinsic pseudocapacitance can be due to either classic surface redox reactions (typically seen in MnO<sub>2</sub> and hydrated RuO<sub>2</sub>) or cation intercalations into bulk materials (for example, T-Nb<sub>2</sub>O<sub>5</sub>) that do not lead to a phase evolution.<sup>[3]</sup> Besides, extrinsic intercalation pseudocapacitive energy storage, which is dependent on material size, with fundamental changes in redox reactions occurring in finite sized systems,<sup>[4]</sup> has also been achieved for some battery-type materials by nanoengineering (for example, MoO<sub>2</sub>, MoS<sub>2</sub>, and

SnS).<sup>[4–6]</sup> While surface redox reactions offer impressive capacitance, they are quite unstable and/or expensive for large-scale applications. Furthermore, such redox reactions occur only on or near the surface, resulting in a low “atom economy.” In contrast, intercalation pseudocapacitance stands out because it can occur within the bulk of the electrode material, and it can provide simultaneously high energy and power densities together with long-term cycling stability. More impressively, the majority of the full theoretical capacity can be accessed within minutes to seconds.<sup>[6]</sup> For example, Dunn and co-workers have demonstrated that a T-Nb<sub>2</sub>O<sub>5</sub> electrode with a thickness of 40 μm could deliver a capacity of 130 mAh g<sup>-1</sup> at a 10C (charge/discharge in 6 min) rate under Li<sup>+</sup> insertion.<sup>[3]</sup> Moreover, a high intercalation capacitance (>300 F cm<sup>-3</sup>) with impressive cycling stability (up to 10 000 cycles) has also been reported by Gogotsi and co-workers in Ti<sub>3</sub>C<sub>2</sub> MXene.<sup>[7]</sup> In fact, a number of metal oxides,<sup>[8,9]</sup> phosphates,<sup>[10]</sup> and sulfides<sup>[11]</sup> have recently been investigated as intercalation pseudocapacitor electrodes.

Among these candidates, brookite phase vanadium oxide, denoted as VO<sub>2</sub> (B), stands out because of its stable open framework, rapid Li<sup>+</sup> (de)intercalation in double layers of V<sub>4</sub>O<sub>10</sub> structure, and high theoretical capacity (323 mAh g<sup>-1</sup> or 1163 C g<sup>-1</sup>).<sup>[12,13]</sup> VO<sub>2</sub> (B) crystallizes in the monoclinic system (C2/m), and its lattice contains chains of perovskite-like cavities interconnected along the *b*-axis through square oxygen-bounded openings; see Figure S1 in the Supporting Information. This arrangement creates a 1D Li<sup>+</sup>-diffusion pathway within VO<sub>2</sub> (B)—parallel to the ⟨010⟩ crystal orientation.<sup>[14,15]</sup>


---

Dr. C. Xia, Dr. C. Zhao, Dr. H. Liang, Prof. H. N. Alshareef  
Materials Science and Engineering  
Physical Sciences and Engineering Division  
King Abdullah University of Science and Technology (KAUST)  
Thuwal 23955-6900, Saudi Arabia  
E-mail: husam.alshareef@kaust.edu.sa

Dr. Z. Lin, Prof. P. Rozier  
CIRIMAT UMR CNRS 5085  
Université Paul Sabatier  
118 route de Narbonne 31062, Toulouse, France

Dr. Z. Lin, Prof. P. Rozier  
Réseau sur le Stockage Electrochimique de l'Energie (RS2E)  
FR CNRS 3459, France

Prof. Y. Zhou, Prof. Z. Wang  
School of Physical Electronics  
University of Electronic Science and Technology of China  
Chengdu 610054, P. R. China

 The ORCID identification number(s) for the author(s) of this article can be found under <https://doi.org/10.1002/adma.201803594>.

DOI: 10.1002/adma.201803594

The electrochemical  $\text{Li}^+$  insertion behavior of  $\text{VO}_2$  (B) was first investigated by Jacobsen and co-workers, who demonstrated that 0.5 Li/V can be inserted at ambient temperature into bulk  $\text{VO}_2$  (B), in a two-phase region at 2.55 V versus Li/Li $^+$ .<sup>[14]</sup> They also pointed out that at higher temperatures, further insertion could be observed in another two-phase region at 2.1 V versus Li/Li $^+$ , and 0.82 Li/V was finally obtained at 120 °C. The  $\text{VO}_2$  (B) lattice generally displays two different types of square pyramidal sites, one of which is feasible for rapid  $\text{Li}^+$  insertion (at 2.5 V vs Li/Li $^+$  at ambient conditions). The other step (at 2.1 V vs Li/Li $^+$ ), however, has extremely slow kinetics. As a result,  $\text{Li}^+$  intercalation capacities of 150 to 200 mAh  $\text{g}^{-1}$  were generally demonstrated, corresponding to 0.46 to 0.62 Li/V.<sup>[13,15–17]</sup> Despite many attempts, the expected high capacity and cycling stability have so far not been experimentally achieved at ambient conditions. For example, Fan and co-workers have reported a hydrothermal process to synthesize vertically aligned  $\text{VO}_2$  (B) nanobelt forest for Li-ion storage. However, the nanobelt forest electrode only shows a limited performance enhancement, which offers a discharge capacity of 178 and 100 mAh  $\text{g}^{-1}$  at 10 and 27 A  $\text{g}^{-1}$ , respectively. The nanobelt electrode suffers 21% capacity decay only after 2000 cycles at a mild charge–discharge rate of 2 A  $\text{g}^{-1}$ .<sup>[18]</sup> Liu and co-workers also reported the  $\text{VO}_2$  (B) array on carbon substrate for Li-ion storage, which only displays a specific capacity of 145 mAh  $\text{g}^{-1}$  at 100 mA  $\text{g}^{-1}$  with unsatisfied cycling stability (10% decay after only 200 cycles at 1 A  $\text{g}^{-1}$ ).<sup>[19]</sup> Furthermore, the previous in situ high-energy synchrotron X-ray diffraction (XRD) study revealed that there was an obvious two-phase transition process for  $\text{VO}_2$  (B) during  $\text{Li}^+$  (de)intercalation,<sup>[15]</sup> which may lead to limited rate capability and cycling stability. Even though the Li-storage performance of  $\text{VO}_2$  (B) can be further enhanced by carbonaceous material decoration,<sup>[20]</sup> boosting the capacitive performance by accelerating the intrinsic, slow kinetics of the  $\text{VO}_2$  (B) has not yet been achieved. However, the latter approach is fundamentally more important as it can break the kinetic limit and thus improve the overall capacity of  $\text{VO}_2$  (B).

Inspired by the recent progress in 2D material development for intercalation pseudocapacitive energy storage,<sup>[8,21,22]</sup> we believe that  $\text{VO}_2$  (B) would also benefit significantly from such 2D architectures (especially atomically thin 2D nanostructures). While the electrochemical performance of atomically thin 2D sheets of  $\text{VO}_2$  (B) has never been reported, there are multiple scientific arguments that make this approach attractive: 1) previous studies demonstrated that the atomically thin 2D geometry displays much lower intercalation energy barriers than the bulk geometry,<sup>[23]</sup> which may make the  $\text{Li}^+$  intercalation step at 2.1 V versus Li/Li $^+$  possible; 2) the ultrahigh surface-to-volume ratio of 2D nanostructures can open up the possibility to introduce extra Li intercalation sites, resulting in higher theoretical capacity in principle; 3) reduced diffusion length leads to enhanced rate capability; and 4) mono- or few-layer 2D  $\text{VO}_2$  (B) may offer a facile 2D lithium-ion diffusion pathway, superior to the 1D diffusion pathway of bulk  $\text{VO}_2$  (B). It is also worthwhile to mention that the charge storage in a quasi-2D process exhibits similar behavior to the surface adsorption mechanism in 2D nanostructures.<sup>[24]</sup> Indeed, our density functional theory (DFT) calculations suggest that the atomically thin 2D nanostructures can greatly lower the  $\text{Li}^+$  intercalation energy barrier

and thus enhance the capacity, as will be discussed later. The key questions are as follows: is whether atomically thin 2D  $\text{VO}_2$  (B) will actually exhibit high rate/high energy properties and how do we experimentally produce atomically thin 2D nanostructures (atomically thin nanosheets) of  $\text{VO}_2$  (B)?

$\text{VO}_2$  (B) is an atypical, layered material, where the layers are linked by strong covalent bonds instead of weak van der Waals interactions. Xie and co-workers demonstrated that through Li ion and large molecule insertion,  $\text{VO}_2$  (B) crystal can be mechanically exfoliated into monolayer atomic sheets, but with low yields that are unsuitable for large-scale energy storage applications.<sup>[25]</sup> The corresponding X-ray absorption fine-structure spectroscopy study revealed that the  $\text{VO}_2$  (B) monolayers could retain their bulk crystal features with subtle structure distortion to decrease the surface energy, and then endow them with thermodynamic stability. In the present paper, we report a new monomer-assisted, self-confined growth strategy to produce atomically thin 2D  $\text{VO}_2$  (B) nanoribbons, and we elucidate their unique electrochemical properties. We demonstrate that the two different types of square pyramidal sites within atomically thin 2D  $\text{VO}_2$  (B) sheets are both highly active for  $\text{Li}^+$  intercalation at room temperature. The intrinsic phase evolution during  $\text{Li}^+$  uptake/removal can be completely suppressed. We also report a high extrinsic intercalation pseudocapacitance of freestanding  $\text{VO}_2$  (B) paper electrodes induced by the atomically thin 2D geometry. A combination of detailed theoretical and experimental methods was used to understand the anomalously large capacity of these atomically thin 2D nanostructures of  $\text{VO}_2$  (B).

The strategy to produce atomically thin 2D nanostructures of  $\text{VO}_2$  (B) relies on the successive intercalation of a 3,4-ethylenedioxythiophene (EDOT) monomer into layered  $\text{V}_2\text{O}_5$  crystal and the sequential space-confined, topotactic in situ reduction of  $\text{V}_2\text{O}_5$ /poly(3,4-ethylenedioxythiophene (PEDOT) organic–inorganic composite, as indicated in Scheme S1 in the Supporting Information. First, we intercalated EDOT monomer into commercial  $\text{V}_2\text{O}_5$  microparticles (**Figure 1A**) at ambient conditions, where the monomer can simultaneously, but gradually, polymerize into PEDOT and significantly expand the interlayer spacing of  $\text{V}_2\text{O}_5$ . The hybrid  $\text{V}_2\text{O}_5$ /PEDOT composite exhibits a nanobelt-like morphology (**Figure 1B**) with lengths of a few tens of micrometers, which can be ascribed to a “silk reeling” type mechanism.<sup>[26]</sup> Then, we produced the atomically thin  $\text{V}_2\text{O}_5$ /PEDOT hybrid composite using ultrasonication, thanks to the dramatically expanded crystal structure. Next, we employed a hydrothermal process to transform such a hybrid composite into  $\text{VO}_2$  (B) in situ. Since the in situ reduction occurs within a PEDOT-confined space, atomically thin 2D samples were finally obtained (**Figure 1C,D**).

The XRD analysis confirms the efficacy of our strategy, as displayed in **Figure 1E** and **Figure S2a** (Supporting Information). It is clear that only two dominant diffraction peaks appear at 4.6° and 9.3° after EDOT intercalation, corresponding to the (001) and (002) peak of  $\text{V}_2\text{O}_5$ /PEDOT hybrid material, respectively. The small-angle XRD scan (**Figure S2a**, Supporting Information) further reveals that the interlayer spacing of  $\text{V}_2\text{O}_5$  significantly expands from 4.3 to 19.2 Å, indicating the insertion of two monolayers of PEDOT between each  $\text{V}_2\text{O}_5$  bilayer.<sup>[27]</sup> X-ray photoelectron spectroscopy (XPS) analysis (**Figure S3**,

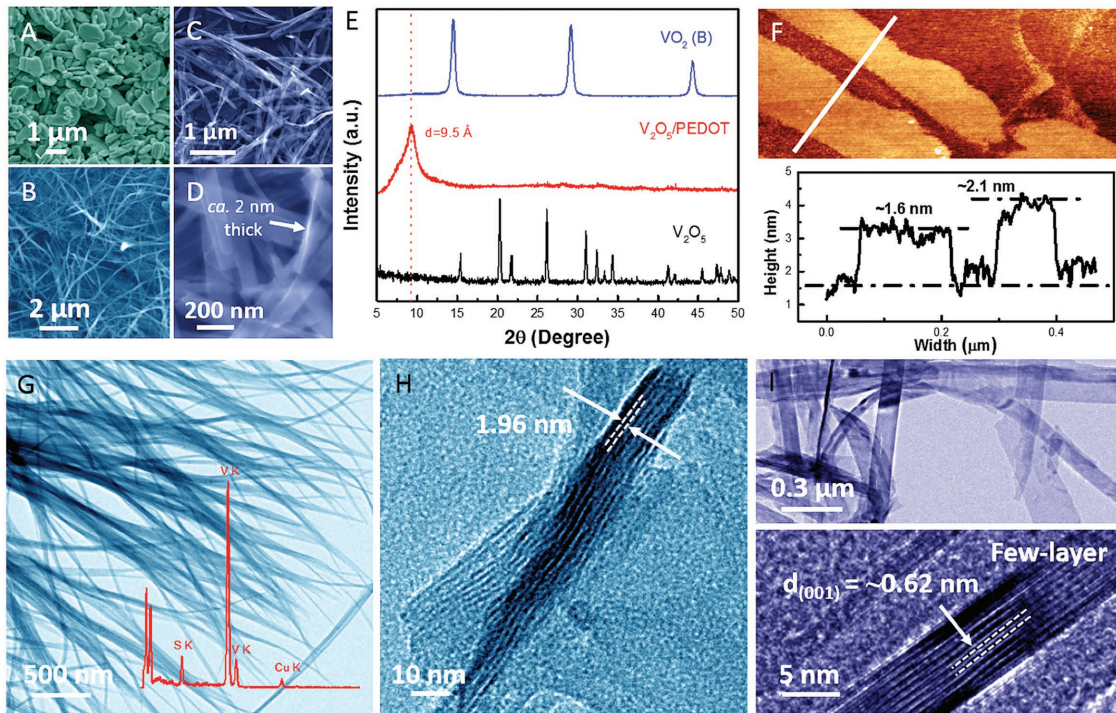


**Figure 1.** Characterization of atomically thin 2D VO<sub>2</sub> (B) nanostructures. A–D) Scanning electron microscopy (SEM) images of A) commercial V<sub>2</sub>O<sub>5</sub> microparticles, B) an as-prepared organic–inorganic V<sub>2</sub>O<sub>5</sub>/PEDOT composite, and C,D) the final product VO<sub>2</sub> (B). E) The typical XRD patterns of V<sub>2</sub>O<sub>5</sub>, a V<sub>2</sub>O<sub>5</sub>/PEDOT composite, and 2D VO<sub>2</sub> (B). F) Representative AFM image of 2D VO<sub>2</sub> (B) nanoribbons, revealing an average thickness of ≈2 nm. G,H) TEM images of hybrid V<sub>2</sub>O<sub>5</sub>/PEDOT composite. The inset in G depicts the EDS spectrum of as-obtained V<sub>2</sub>O<sub>5</sub>/PEDOT, demonstrating the coexistence of S and V elements. I) HRTEM images of 2D VO<sub>2</sub> (B) nanoribbons.

Supporting Information) shows that V<sup>5+</sup> component is the dominated specie at V<sub>2</sub>O<sub>5</sub>/PEDOT surface, implying the successful retention of V<sub>2</sub>O<sub>5</sub> structure in V<sub>2</sub>O<sub>5</sub>/PEDOT. After transforming to VO<sub>2</sub> (B), only the diffraction peaks from (00 $l$ ) planes were observed, confirming the mono- or few-layer nature of 2D VO<sub>2</sub> (B).<sup>[25]</sup> In addition, we further proved that the intercalation and sonication steps are indispensable to obtaining atomically thin 2D VO<sub>2</sub> (B) nanostructures (see detailed discussion in Note S1 in the Supporting Information). The atomic force microscopy (AFM) study also illustrates the flat and atomically thin nature of VO<sub>2</sub> (B) (≈2 nm thick; Figure 1F). Our Raman study supports the existence of PEDOT polymer—the Raman signatures at 1263, 1366, 1453, 1502, and 1569 cm<sup>-1</sup> originate from the PEDOT polymer, accounting for 37.3 wt% in the 2D VO<sub>2</sub> (B)/PEDOT composite (Figure S2c and Note S2, Supporting Information). The transmission electron microscopy (TEM) and energy-dispersive X-ray spectroscopy (EDS) analyses further support the successful intercalation of PEDOT into a V<sub>2</sub>O<sub>5</sub> lattice, showing the coexistence of S and V elements and a 1.96 nm interlayer spacing of the V<sub>2</sub>O<sub>5</sub>/PEDOT composite (Figure 1G,H). These observations are consistent with our XRD data. Moreover, the lattice-resolved, high-resolution TEM (HRTEM) image of the edge of an individual 2D VO<sub>2</sub> (B) ribbon displays a spacing of ≈0.62 nm, which matches the  $d$ -spacing of the (001) planes (Figure 1I). This set of planes runs parallel to the thickness of the ribbon, revealing as-prepared 2D VO<sub>2</sub> (B) nanoribbon with a thickness of a few layers. It is notable that these as-obtained VO<sub>2</sub> (B) samples still demonstrate a single-crystallinity character despite their

atomically thin nature (Figure S2d, Supporting Information). In addition, the HRTEM and EDS measurements show that the as-prepared atomically thin 2D VO<sub>2</sub> (B) exhibits clear surface without PEDOT coating (Figure S4, Supporting Information). While the residual PEDOT may randomly disperse within atomically-thin 2D VO<sub>2</sub> (B) nanoribbons, they do not contribute to the Li-ion storage performance, as demonstrated later.

Self-supported VO<sub>2</sub> (B) membrane was fabricated to serve as the working electrode for electrochemical study. Under the galvanostatic condition of a 0.5C rate, the electrochemical profiles representing Li<sup>+</sup> (de)intercalation into atomically thin 2D VO<sub>2</sub> (B) hosts are presented in Figure 2A. Note that our control experiments reveal that the capacity contribution from PEDOT is considerably limited (13 mAh g<sup>-1</sup>; Figure S5a,b, Supporting Information). As presented in Figure 2A, at 0.5C, a high capacity of approximately 550 mAh g<sup>-1</sup> (1210 μAh cm<sup>-2</sup>) is obtained for the atomically thin 2D VO<sub>2</sub> (B) electrode with a thickness of 50–60 μm, corresponding to a 1.7 electron redox reaction. The charge–discharge profiles are seen as sloping types over the entire voltage range, except around 2.5 V where a plateau (capacity contribution at plateau region: ≈150 mAh g<sup>-1</sup>) is observed. This observation implies that ≈27% Li is inserted into VO<sub>2</sub> (B) tunnels and ≈73% Li ions intercalated onto the atomically thin VO<sub>2</sub> (B) surface at 0.5C. The predominantly sloping charge–discharge profiles suggest that a solid-solution type process is associated with Li<sup>+</sup> intercalation. However, in contrast to our atomically thin 2D sample, the previous reports show that over 70% capacity of bulk and nanosized

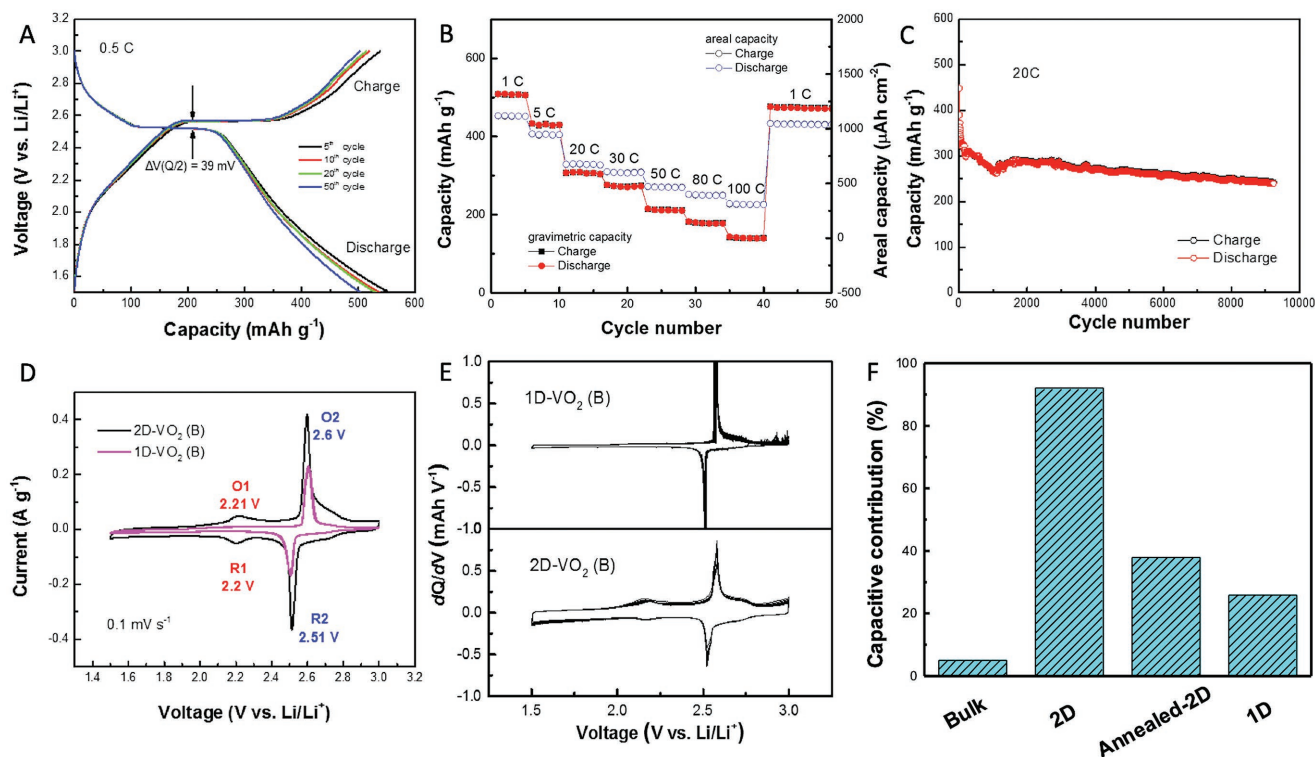


**Figure 2.** Electrochemical behavior of atomically thin 2D VO<sub>2</sub> (B) nanostructures. A) Galvanostatic charge–discharge profiles for atomically thin 2D VO<sub>2</sub> (B) electrodes at 0.5C. B) Rate capability of atomically thin 2D VO<sub>2</sub> (B) electrodes. C) Cycle performances at a current rate of 20C. D) Voltammetry sweeps at 0.1 mV s<sup>-1</sup>. E) Differential capacity plots at 1C for 1D and atomically thin 2D VO<sub>2</sub> (B). F) Normalized contribution ratio of capacitive contribution to current for different VO<sub>2</sub> (B) electrodes.

VO<sub>2</sub> (B) comes from the two-phase plateau region (Figure S6, Supporting Information). Impressively, the overpotential—the difference between the charge and discharge potential at the half reversible capacity—of our VO<sub>2</sub> (B) electrode is a mere 39 mV, outperforming all previously reported VO<sub>2</sub> (B) nanostructures,<sup>[13,16,28]</sup> and indicating higher electrical and ionic conductivity. The rate performance of these 2D electrodes was also investigated. The good rate capability of atomically thin 2D VO<sub>2</sub> (B) is illustrated in Figure 2B, where the current density was increased step-wise from 1C to 100C and then returned to 1C. The measured capacities at 1C, 5C, 20C, 30C, 50C, 80C, and 100C were 506, 429, 303, 275, 212, 179, and 140 mAh g<sup>-1</sup> respectively. It is of note that the capacity of these 2D electrodes recovered to 470 mAh g<sup>-1</sup> when the current density was returned to 1C. The strong dependence on C-rate for Li capacity is probably due to the ultrathick nature of our tested membranes (50–60 μm). The similar phenomenon was also observed in MXene papers.<sup>[29]</sup> Gogosti et al. showed that the volumetric capacitance of 40 μm thick MXene hydrogel film electrode shows much stronger dependence on scan rates than 13 and 3 μm thick electrodes. Of note, the obtained high capacity at high C-rate (e.g., 303 mAh g<sup>-1</sup> at 20C) of our atomically thin VO<sub>2</sub> (B) is among the best in existing literature. For example, Duan et al. reported a nice study on 3D-graphene/Nb<sub>2</sub>O<sub>5</sub> composite, achieving a Li-capacity of ≈150 mAh g<sup>-1</sup> at 10C.<sup>[29,30]</sup> Dunn and co-workers showed a nano-sized-MoO<sub>2</sub> electrode with capacity of 120 mAh g<sup>-1</sup> at 10C.<sup>[4]</sup> Tolbert and co-workers reported a MoS<sub>2</sub> electrode with Li-intercalation capacity of 150 mAh g<sup>-1</sup> at 23C.<sup>[31]</sup> We further

demonstrate that these 2D electrodes exhibit ultrastable lithiation/delithiation over at least 1300 cycles at a current density of 0.1C (Figure S5c, Supporting Information). Even when cycled at 20C, the atomically thin 2D VO<sub>2</sub> (B) nanoribbons do not display a notable capacity decay after 9000 cycles (Figure 2C). It is worthwhile to note that Coulombic efficiency during cycling tests is close to 100%, confirming that the outstanding performance is not due to parasitic reactions.<sup>[21]</sup>

Cyclic voltammetry (CV) measurements were used to further characterize the electrochemical behavior of as-prepared samples. As depicted in Figure 2D, it is interesting that two distinct pairs of peaks at around 2.21/2.2 V (O1/R1) and 2.6/2.51 V (O2/R2) are observed in atomically thin 2D VO<sub>2</sub> (B) electrodes at room temperature. In sharp contrast, we only observed one redox peak (at 2.5 V vs Li/Li<sup>+</sup>, which is also commonly seen in the literature) for the 1D VO<sub>2</sub> (B) nanowire control sample. The lack of the redox peaks at ≈2.1 V versus Li/Li<sup>+</sup> results in a much lower capacity. Note that the electrochemical behavior of the VO<sub>2</sub> (B) nanowires is actually quite similar to that of bulk VO<sub>2</sub> (B), indicating that such 1D geometry may offer a faster electron transfer pathway; however, it does not overcome the intrinsic, sluggish kinetics and only demonstrates limited enhancement, as compared to the bulk VO<sub>2</sub> (B). The newly evolved couple of CV peaks (O1/R1) that we observed in our atomically thin 2D VO<sub>2</sub> (B) has never been seen in various VO<sub>2</sub> (B) nanostructures at room temperature. Therefore, we believe that the atomically thin 2D nanostructures can greatly lower the lithiation energy barrier of

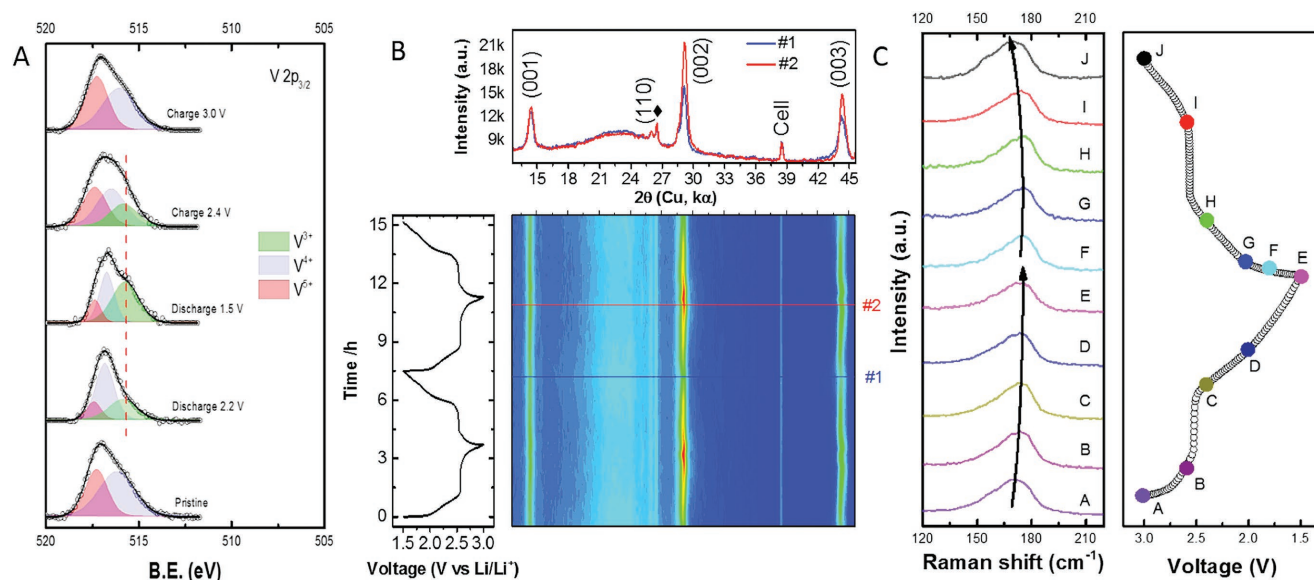


**Figure 3.** Structural characterizations of the atomically thin 2D VO<sub>2</sub> (B) during electrochemical cycling. A) Ex situ high-resolution XPS spectra of the V 2p<sub>3/2</sub> region in pristine, lithiated (2.2 and 1.5 V) and delithiated (2.4 and 3 V) atomically thin 2D VO<sub>2</sub> (B) electrodes. B) Operando XRD measurement for atomically thin 2D electrode. Note that the rhombus marked peak at ≈26° originates from our multiwall CNT additive. C) In situ Raman spectra from atomically thin 2D VO<sub>2</sub> (B) electrodes recorded during the second cycle as a function of depth of discharge and charge.

the kinetically sluggish step (at 2.1 V vs Li/Li<sup>+</sup>), which could only be achieved at high temperatures in all previous studies. It is also worth mentioning that this process is highly reversible, since no measurable peak current losses are observed even after continuous 200 CV cycles (Figure S5d, Supporting Information). This result indicates that the two different types of square pyramidal sites in atomically thin 2D VO<sub>2</sub> (B) are both highly active and stable for Li<sup>+</sup> intercalation at ambient conditions. These observations have driven us to further investigate the origin of such differences between our atomically thin 2D VO<sub>2</sub> (B) and other nanostructured VO<sub>2</sub> (B) (for example, 1D nanowires). We therefore carried out the differential capacity analysis, as presented in Figure 2E and Figure S5e (Supporting Information, which display the differential capacity plots of the 1D and 2D VO<sub>2</sub> (B) electrodes. The results demonstrate that the capacity contribution of 1D VO<sub>2</sub> (B) originates mainly from a narrow region at ≈2.5 V versus Li/Li<sup>+</sup>, while the capacity contribution of 2D VO<sub>2</sub> (B) stems from the entire voltage window. Additionally, the perfectly reproducible differential capacity curves of 2D electrodes, with clear oxidation and reduction peaks, illustrate their excellent reversibility during Li<sup>+</sup> uptake/removal. The high charge transfer resistance of a VO<sub>2</sub> (B) electrode is a key factor that limits its long-term cycling stability for Li storage.<sup>[32]</sup> The significantly reduced charge-transfer resistance of atomically thin 2D VO<sub>2</sub> (B) is evidence of enhanced cycling performance (Figure S5f, Supporting Information).

To understand the charge storage kinetics in atomically thin 2D VO<sub>2</sub> (B), we quantified the pseudocapacitive and diffusion limited contributions to the total capacity, using the previously reported approach by Dunn and co-workers<sup>[33]</sup> The 1D, Ar-annealed, atomically thin 2D and bulk VO<sub>2</sub> (B) are included for comparison. The results, summarized in Figure 2F, indicate that at a scan rate of 0.3 mV s<sup>-1</sup>, the 1D, annealed, atomically

thin 2D and bulk VO<sub>2</sub> (B) demonstrate a 26%, 38%, and 4.9% capacitive contribution respectively. However, 92% of the current can be attributed to the capacitive response of the atomically thin 2D VO<sub>2</sub> (B) sheets, clearly revealing a much higher level of pseudocapacitive charge storage by geometry tuning. It is especially important to note that when the unique, atomically thin 2D structure of VO<sub>2</sub> (B) is destroyed by Ar annealing at the evaluated temperature (Figure 2F, Annealed-2D), a dramatic decrease in the fraction of capacitor-like current is observed. This strongly demonstrates that the atomically thin 2D feature is crucial for achieving high pseudocapacitive performance in VO<sub>2</sub> (B).

To gain insight into the electrochemical intercalation process in the atomically thin 2D VO<sub>2</sub> (B) host, an ex situ XRD analysis was first carried out. Figure S7a (Supporting Information) depicts Bragg peaks corresponding to the 2D VO<sub>2</sub> (B) phase at different charge or discharge states in the second cycle. Atomically thin 2D VO<sub>2</sub> (B) obviously does not undergo a phase evolution following (de)lithiation. Also, no peak shifting of the (00l) diffraction peaks is observed, indicating minimal structural modification of 2D VO<sub>2</sub> (B) upon Li<sup>+</sup> uptake/removal. This behavior exhibits electrochemical signatures that are representative of intercalation pseudocapacitance. The ex situ XPS analysis provides further proof of reversible Li<sup>+</sup> intercalation, as illustrated in Figure 3A. The pristine 2D VO<sub>2</sub> (B) electrodes demonstrate V 2p<sub>3/2</sub> at 516.1 and 517.3 eV, corresponding to V<sup>4+</sup> and V<sup>5+</sup> species respectively.<sup>[34,35]</sup> A new V 2p<sub>3/2</sub> feature (515.6 eV), namely V<sup>3+</sup>, appears upon discharge.<sup>[35]</sup> The V<sup>3+</sup> signal apparently increases in intensity upon continued discharge. However, the V<sup>3+</sup> contribution is gradually diminished upon charging, and the pristine V 2p<sub>3/2</sub> is almost regenerated following delithiation to 3.0 V, confirming the reversibility and stability of these 2D VO<sub>2</sub> (B) sheets (see Note S3 in the Supporting Information for details).

The detailed charge storage mechanism in VO<sub>2</sub> (B) electrodes were investigated using “Operando” XRD analysis. Figure S7b (Supporting Information) illustrates the structural evolutions accompanying the Li<sup>+</sup> (de)intercalation of thick VO<sub>2</sub> (B) nanoribbons (~20–40 nm; Figure S8, Supporting Information), which is employed as control sample. The electrochemical profile shows a biphasic process indicating that XRD pattern #1 and #2 are characteristic of the high Li content (discharged state) phase and low Li content (charged state) phase, respectively. In both patterns, only (00*l*) peaks together with (110), (−401), and (310) peaks are observed, in agreement with the nanoribbon-like shape of the sample. Upon Li<sup>+</sup> intercalation, (110) and (310) peaks shift toward low Bragg angles, indicating an increase of the *b* cell parameter of lithiated phase compared to the pristine VO<sub>2</sub> (B). A slight shift of (00*l*) peaks can be seen as well, which corresponds to a slightly larger *c* cell parameter of lithiated phase. Pristine and lithiated phases coexist during the charge/discharge plateau at 2.5 V, such as observed in battery-like intercalation reactions. While the phase change process appears to be reversible, as most intercalation processes, it is also kinetically limited thus leading to an intrinsically poor Li-storage performance such as limited rate capability. It is noteworthy that thick VO<sub>2</sub> (B) electrode exhibits a polarization of 126 mV, which is close to the reported nanostructured and bulk VO<sub>2</sub> (B). Therefore, it is clear that the nanostructured VO<sub>2</sub> (B) displays a similar mechanism to its bulk counterparts,<sup>[15]</sup> and it cannot break the intrinsic kinetic limit. Our atomically thin 2D VO<sub>2</sub> (B) material shows a different mechanism. As illustrated in Figure 3B, no noticeable evolution of the XRD patterns is observed upon discharge/charge. More importantly, at the voltage plateau, the sudden split of the (110) peak did not occur, revealing the successful tuning of battery-like Li insertion mechanism for VO<sub>2</sub> (B). The reversible change in intensity is assumed to come from a reversible disordering—reordering process along cycling associated with the huge amount of capacity at nonplateau part (Figure 2A). Further, a polarization of 46 mV for 2D electrodes is observed in our Operando cells, suggesting faster kinetics compared to the thick VO<sub>2</sub> electrode. In summary, the Operando tests successfully reveal that atomically thin 2D geometry breaks the intrinsic kinetic limit of bulk materials, leading to enhanced electrochemical kinetic associated with an extrinsic pseudocapacitive behavior.

Furthermore, an in situ Raman study was employed to confirm the high reversibility of our atomically thin 2D electrode. In situ Raman microscopy spectra, obtained from an atomically thin 2D VO<sub>2</sub> (B) electrode recorded during the galvanostatic discharge, and the subsequent charge scan in the second cycle are presented in Figure S9 in the Supporting Information. At the open-circuit voltage (≈3.13 V), the A<sub>g</sub> mode of atomically thin 2D VO<sub>2</sub> (B) is located at ≈171 cm<sup>−1</sup>, corresponding to the V–O–V bending, which is good and consistent with previous reports.<sup>[36]</sup> The peaks at 715 and 892 cm<sup>−1</sup> are associated with an O=C ring-bending mode and a symmetric ring-breathing mode of ethylene carbonate respectively. The peak at 900 cm<sup>−1</sup> corresponds to the CH<sub>3</sub>–O stretching of diethyl carbonate. In addition, the totally symmetric vibration mode of the PF<sub>6</sub><sup>−</sup> anion is located at 746 cm<sup>−1</sup>.<sup>[37]</sup> During the entire charge–discharge (CD) scan, no new peaks are observed, implying that no new phase is formed. Figure 3C displays the evolution of the A<sub>g</sub>

peak of the 2D electrode in detail, demonstrating that none of the Raman peaks vanish during the CD test. The redshift of the A<sub>g</sub> mode upon discharge probably originates from the partial regeneration of the local V–O polyhedra,<sup>[38]</sup> but without crystallographic transformation. The extraction of lithium atoms returns the structure of Li<sub>σ</sub>VO<sub>2</sub> (B) to that of pristine 2D VO<sub>2</sub> (B). These findings match with those deduced from the operando XRD and ex situ XPS studies: the atomically thin 2D VO<sub>2</sub> (B) nanoribbons intercalate Li<sup>+</sup> ions with unobservable lattice expansion.

The above results demonstrate that the atomically thin 2D VO<sub>2</sub> (B) electrode yields a higher capacity (much beyond the theoretical capacity of its bulk analogue) and faster kinetics than those that can be achieved in other VO<sub>2</sub> (B) nanostructures. We used the DFT calculations to gain greater insight into this phenomenon. Figure 4A,B displays the atomic arrangements in the structure of bulk VO<sub>2</sub> (B) and a monolayer of 2D VO<sub>2</sub> (B). We then calculated the corresponding phonon dispersion curves to check the stability of the monolayer 2D VO<sub>2</sub> (B). As Figure 4C illustrates, all vibrational modes are real in the whole Brillouin zone, indicating that the 2D VO<sub>2</sub> (B) monolayer is kinetically stable. Our calculations demonstrate that Li ions can bind to four unique sites in a VO<sub>2</sub> (B) cell with adsorption energies of −2.19, −2.28, −2.51, and −2.57 eV for bulk samples (Figure S10, Supporting Information), which are in good agreement with previous studies.<sup>[12]</sup> The theoretical maximum capacity of bulk VO<sub>2</sub> (B) is ≈403 mAh g<sup>−1</sup>, corresponding to Li<sub>1.25</sub>VO<sub>2</sub> (B). However, the 2D VO<sub>2</sub> (B) monolayer has significantly reduced energy barriers for Li<sup>+</sup> adsorption. In this configuration, the adsorption energies are −2.25, −2.69, −2.81, and −2.87 eV (Figure 4D), suggesting faster kinetics. The much lower intercalation barriers of atomically thin 2D VO<sub>2</sub> (B) nanostructures lead to the appearance of the O1/R1 redox peak at room temperature. More interestingly, as displayed in Figure 4E, we found that the theoretical Li-ion intercalation capacity of monolayer 2D VO<sub>2</sub> (B) is ≈884 mAh g<sup>−1</sup> (3 Li/V can be inserted), which is more than twice that of bulk VO<sub>2</sub> (B). This is why we can experimentally achieve a Li<sup>+</sup> intercalation capacity of 550 mAh g<sup>−1</sup> at 0.5C using these atomically thin 2D VO<sub>2</sub> (B) electrodes. The theoretical results indicate that 25% Li is insertion and 75% Li binds to the atomically thin 2D VO<sub>2</sub> (B) surface when 2 Li/V (≈590 mAh g<sup>−1</sup>) is reached, which is consistent with our experimental measurements. Furthermore, as shown in Figure S11 (Supporting Information), our DFT results demonstrate that a slight disordering process will occur after heavy Li<sup>+</sup> intercalation (beyond 1.5 Li/V). While the crystal skeleton of 2D VO<sub>2</sub> (B) can be maintained, the distortion of V–O bonds is clearly observed. These partially disordered structures in 2D VO<sub>2</sub> (B) will decrease the intensities of its XRD peaks, in good agreement with our Operando XRD analysis. The lithium dynamic process was revealed using the Li<sup>+</sup>-diffusion energy barrier along various trajectories. The most possible diffusion pathways of monolayer 2D VO<sub>2</sub> (B) is provided in Figure S12 in the Supporting Information. The calculated energy barriers of Li<sup>+</sup> diffusion along P1, P2, and P3 directions (Figure 4F–H) are 190, 204, and 181 meV respectively. On the other hand, we demonstrate that the Li<sup>+</sup>-diffusion barriers of bulk VO<sub>2</sub> (B) are 270 (along the *b* axis) and 927 meV (along the *a* axis), as indicated in Figure S10 in the Supporting Information. The DFT calculations confirm that the



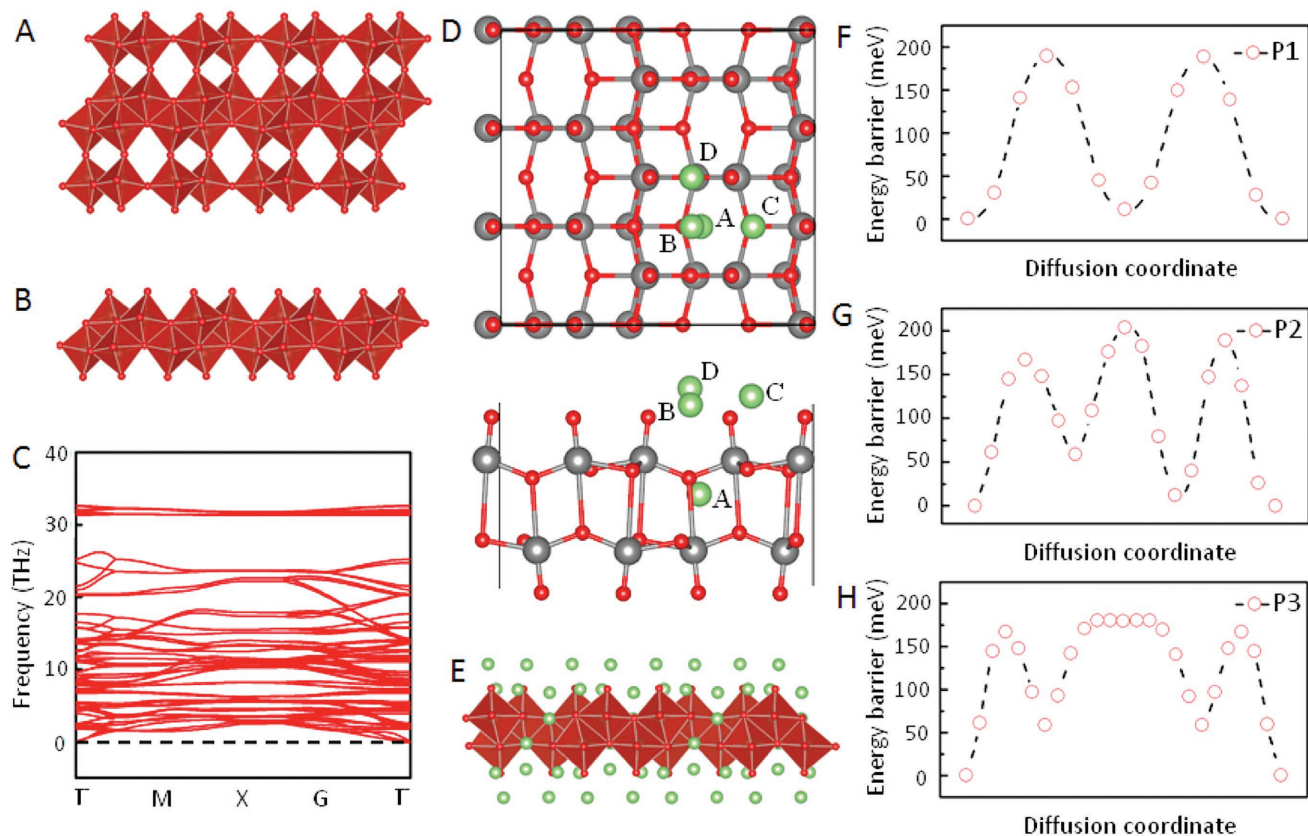


**Figure 4.** Theoretical calculations of 2D VO<sub>2</sub> (B) monolayers for Li-ion storage. A, B) The atomic arrangements in the structure of VO<sub>2</sub> (B) bulk and 2D VO<sub>2</sub> (B) monolayers respectively. The red polyhedra in panels (A) and (B) represent VO<sub>6</sub> octahedra. C) The DFT calculated phonon dispersion curves of monolayer 2D VO<sub>2</sub> (B). D) The possible Li intercalation sites of monolayer 2D VO<sub>2</sub> (B). The red, gray, and green atoms represent O, V, and Li respectively. E) The stable Li-intercalated structure of monolayer 2D VO<sub>2</sub> (B), which demonstrates a theoretical capacity of 884 mAh g<sup>-1</sup> for Li-ion storage. The red polyhedra and the green atoms in panel (E) represent VO<sub>6</sub> octahedra and the lithium atoms. F–H) The representative Li diffusion energy profile along the various trajectories. Note that the diffusion pathways are illustrated in Figure S12 in the Supporting Information.

Li atom diffusion in bulk VO<sub>2</sub> (B) occurs predominantly along the *b* axis. Conversely, low Li<sup>+</sup>-diffusion barriers are calculated along different trajectories in 2D VO<sub>2</sub> (B), revealing its quasi-2D energy storage behavior, which is responsible for the high rate capability. Furthermore, the lower intercalation energy and Li<sup>+</sup>-diffusion barriers lead to subtle structural modifications in atomically thin 2D VO<sub>2</sub> (B) upon lithium-ion insertion/extraction, resulting in enhanced cycling stability.

In this work, we proposed a simple strategy to produce high-quality, atomically thin 2D VO<sub>2</sub> (B) sheets for pseudocapacitive energy storage. It is demonstrated that by engineering the nanostructure, intercalation pseudocapacitance can be significantly enhanced. In addition, we have demonstrated that there are no diffusion limitations to Li in atomically thin 2D VO<sub>2</sub> (B) nanoribbon themselves. Even at charge-discharge rate as fast as 100C (36 s), these 2D electrodes still offer a high capacity of 140 mAh g<sup>-1</sup> due to the rapid Li<sup>+</sup> ion diffusion in these 2D sheets. Moreover, the unique atomically thin 2D structure also enables exceptional areal capacity of 1210 and 667 μAh cm<sup>-2</sup> for a 50 μm thick electrode at 0.5C and 20C, respectively. Furthermore, the atomically thin 2D feature can strongly decrease the intercalation energy of Li<sup>+</sup> into VO<sub>2</sub> (B) crystal, and it can reduce Li diffusion barriers. The absence of any phase

transition, together with the sweep voltammetry analysis, support our hypothesis that a Li<sup>+</sup> intercalation pseudocapacitive mechanism dominates in atomically thin 2D VO<sub>2</sub> (B). These results suggest that the atomically thin 2D geometry of non-van der Waals layered materials could lead to significantly enhanced pseudocapacitive performance.

## Experimental Section

Experimental details are included in the Supporting Information.

## Supporting Information

Supporting Information is available from the Wiley Online Library or from the author.

## Acknowledgements

C.X., Z.L., and Y.Z. contributed equally to this work. Research reported in this publication was supported by King Abdullah University of Science and Technology (KAUST). C.X. acknowledges support from Fan Zhang

and Jing Guo at KAUST. The authors like to also thank Professor Bruce Dunn, UCLA, and Professor Patrice Simon, Université Paul Sabatier, for useful discussions.

## Conflict of Interest

The authors declare no conflict of interest.

## Keywords

2D, intercalation, kinetic barrier, pseudocapacitance, ultrathin

Received: June 6, 2018

Revised: July 24, 2018

Published online: August 30, 2018

- 
- [1] a) P. Simon, Y. Gogotsi, *Nat. Mater.* **2008**, *7*, 845; b) B. Dunn, H. Kamath, J.-M. Tarascon, *Science* **2011**, *334*, 928.
- [2] M. R. Lukatskaya, B. Dunn, Y. Gogotsi, *Nat. Commun.* **2016**, *7*, 12647.
- [3] V. Augustyn, J. Come, M. A. Lowe, J. W. Kim, P.-L. Taberna, S. H. Tolbert, H. D. Abruña, P. Simon, B. Dunn, *Nat. Mater.* **2013**, *12*, 518.
- [4] H.-S. Kim, J. B. Cook, S. H. Tolbert, B. Dunn, *J. Electrochem. Soc.* **2015**, *162*, A5083.
- [5] a) Q. Mahmood, S. K. Park, K. D. Kwon, S. J. Chang, J. Y. Hong, G. Shen, Y. M. Jung, T. J. Park, S. W. Khang, W. S. Kim, *Adv. Energy Mater.* **2016**, *6*, 1501115; b) D. Chao, C. Zhu, P. Yang, X. Xia, J. Liu, J. Wang, X. Fan, S. V. Savilov, J. Lin, H. J. Fan, *Nat. Commun.* **2016**, *7*, 12122.
- [6] J. B. Cook, H. S. Kim, T. C. Lin, C. H. Lai, B. Dunn, S. H. Tolbert, *Adv. Energy Mater.* **2017**, *7*, 1601283.
- [7] M. R. Lukatskaya, O. Mashtalir, C. E. Ren, Y. Dall'Agnese, P. Rozier, P. L. Taberna, M. Naguib, P. Simon, M. W. Barsoum, Y. Gogotsi, *Science* **2013**, *341*, 1502.
- [8] H.-S. Kim, J. B. Cook, H. Lin, J. S. Ko, S. H. Tolbert, V. Ozolins, B. Dunn, *Nat. Mater.* **2017**, *16*, 454.
- [9] D. Chao, C. H. Lai, P. Liang, Q. Wei, Y. S. Wang, C. Zhu, G. Deng, V. V. Doan-Nguyen, J. Lin, L. Mai, *Adv. Energy Mater.* **2018**, *8*, 1800058.
- [10] Y. Zhu, L. Peng, D. Chen, G. Yu, *Nano Lett.* **2015**, *16*, 742.
- [11] G. A. Muller, J. B. Cook, H.-S. Kim, S. H. Tolbert, B. Dunn, *Nano Lett.* **2015**, *15*, 1911.
- [12] S. Lee, X.-G. Sun, A. A. Lubimtsev, X. Gao, P. Ganesh, T. Z. Ward, G. Eres, M. F. Chisholm, S. Dai, H. N. Lee, *Nano Lett.* **2017**, *17*, 2229.
- [13] C. Niu, J. Meng, C. Han, K. Zhao, M. Yan, L. Mai, *Nano Lett.* **2014**, *14*, 2873.
- [14] B. Zachau-Christiansen, K. West, T. Jacobsen, *Mater. Res. Bull.* **1985**, *20*, 485.
- [15] Q. Liu, G. Tan, P. Wang, S. C. Abeyweera, D. Zhang, Y. Rong, Y. A. Wu, J. Lu, C.-J. Sun, Y. Ren, *Nano Energy* **2017**, *36*, 197.
- [16] L. Mai, Q. Wei, Q. An, X. Tian, Y. Zhao, X. Xu, L. Xu, L. Chang, Q. Zhang, *Adv. Mater.* **2013**, *25*, 2969.
- [17] P. Liu, Y. Xu, K. Zhu, K. Bian, J. Wang, X. Sun, Y. Gao, H. Luo, L. Lu, J. Liu, *J. Mater. Chem. A* **2017**, *5*, 8307.
- [18] G. Ren, M. N. F. Hoque, X. Pan, J. Warzywoda, Z. Fan, *J. Mater. Chem. A* **2015**, *3*, 10787.
- [19] S. Li, G. Liu, J. Liu, Y. Lu, Q. Yang, L.-Y. Yang, H.-R. Yang, S. Liu, M. Lei, M. Han, *J. Mater. Chem. A* **2016**, *4*, 6426.
- [20] C. Nethravathi, C. R. Rajamathi, M. Rajamathi, U. K. Gautam, X. Wang, D. Golberg, Y. Bando, *ACS Appl. Mater. Interfaces* **2013**, *5*, 2708.
- [21] M. Ghidui, M. R. Lukatskaya, M.-Q. Zhao, Y. Gogotsi, M. W. Barsoum, *Nature* **2014**, *516*, 78.
- [22] S. Fleischmann, D. Leistenschneider, V. Lemkova, B. Krüner, M. Zeiger, L. Borchardt, V. Presser, *Chem. Mater.* **2017**, *29*, 8653.
- [23] a) Y. Zheng, T. Zhou, X. Zhao, W. K. Pang, H. Gao, S. Li, Z. Zhou, H. Liu, Z. Guo, *Adv. Mater.* **2017**, *29*, 1700396; b) G. A. Tritsaris, E. Kaxiras, S. Meng, E. Wang, *Nano Lett.* **2013**, *13*, 2258.
- [24] B. E. Conway, *J. Electrochem. Soc.* **1991**, *138*, 1539.
- [25] L. Liu, T. Yao, X. Tan, Q. Liu, Z. Wang, D. Shen, Z. Sun, S. Wei, Y. Xie, *Small* **2012**, *8*, 3752.
- [26] C. X. Guo, K. Sun, J. Ouyang, X. Lu, *Chem. Mater.* **2015**, *27*, 5813.
- [27] A. V. Murugan, B. Kale, C.-W. Kwon, G. Campet, K. Vijayamohanam, *J. Mater. Chem.* **2001**, *11*, 2470.
- [28] a) D. Chao, C. Zhu, X. Xia, J. Liu, X. Zhang, J. Wang, P. Liang, J. Lin, H. Zhang, Z. X. Shen, *Nano Lett.* **2014**, *15*, 565; b) S. Yang, Y. Gong, Z. Liu, L. Zhan, D. P. Hashim, L. Ma, R. Vajtai, P. M. Ajayan, *Nano Lett.* **2013**, *13*, 1596.
- [29] M. R. Lukatskaya, S. Kota, Z. Lin, M.-Q. Zhao, N. Shpigel, M. D. Levi, J. Halim, P.-L. Taberna, M. W. Barsoum, P. Simon, Y. Gogotsi, *Nat. Energy* **2017**, *2*, 17105.
- [30] H. Sun, L. Mei, J. Liang, Z. Zhao, C. Lee, H. Fei, M. Ding, J. Lau, M. Li, C. Wang, X. Xu, G. Hao, B. Papandrea, I. Shakir, B. Dunn, Y. Huang, X. Duan, *Science* **2017**, *356*, 599.
- [31] J. B. Cook, H. S. Kim, Y. Yan, J. S. Ko, S. Robbennolt, B. Dunn, S. H. Tolbert, *Adv. Energy Mater.* **2016**, *6*, 1501937.
- [32] Q. Zhao, L. Jiao, W. Peng, H. Gao, J. Yang, Q. Wang, H. Du, L. Li, Z. Qi, Y. Si, *J. Power Sources* **2012**, *199*, 350.
- [33] J. Wang, J. Polleux, J. Lim, B. Dunn, *J. Phys. Chem. C* **2007**, *111*, 14925.
- [34] J. Jeong, N. Aetukuri, T. Graf, T. D. Schladt, M. G. Samant, S. S. Parkin, *Science* **2013**, *339*, 1402.
- [35] M. A. Eberhardt, A. Proctor, M. Houalla, D. M. Hercules, *J. Catal.* **1996**, *160*, 27.
- [36] S. Ni, H. Zeng, X. Yang, *J. Nanomater.* **2011**, *2011*, 3.
- [37] D. Chao, P. Liang, Z. Chen, L. Bai, H. Shen, X. Liu, X. Xia, Y. Zhao, S. V. Savilov, J. Lin, *ACS Nano* **2016**, *10*, 10211.
- [38] X. Zhang, R. Frech, *J. Electrochem. Soc.* **1998**, *145*, 847.